Published in final edited form as:

Dev Neurosci. 2017 ; 39(5): 399–412. doi:10.1159/000471509.

Maternal Inflammation Results in Altered Tryptophan Metabolism in Rabbit Placenta and Fetal Brain

Monica Williams[#a], **Zhi Zhang**[#a], **Elizabeth Nance**[a], **Julia L. Drewes**[c], **Wojciech G. Lesniak**[b], **Sarabdeep Singh**[a], **Diane C. Chugani**[d,e], **Kannan Rangaramanujam**[b], **David R. Graham**[c], and **Sujatha Kannan**[a]

[a]Department of Anesthesiology and Critical Care Medicine, Johns Hopkins University SOM, Baltimore, MD

[b]Center for Nanomedicine, Wilmer Eye Institute, Johns Hopkins University SOM, Baltimore, MD

[c]Department of Molecular and Comparative Pathobiology, Johns Hopkins University SOM, Baltimore, MD

[d]Nemours/AI duPont Hospital for Children, Wilmington, DE

[e]Communication Sciences and Disorders Department, College of Health Sciences, University of Delaware, Newark, DE, USA

[#] These authors contributed equally to this work.

Abstract

Maternal inflammation has been linked to neurodevelopmental and neuropsychiatric disorders such as cerebral palsy, schizophrenia, and autism. We had previously shown that intrauterine inflammation resulted in a decrease in serotonin, one of the tryptophan metabolites, and a decrease in serotonin fibers in the sensory cortex of newborns in a rabbit model of cerebral palsy. In this study, we hypothesized that maternal inflammation results in alterations in tryptophan pathway enzymes and metabolites in the placenta and fetal brain. We found that intrauterine endotoxin administration at gestational day 28 (G28) resulted in a significant upregulation of indoleamine 2,3-dioxygenase (IDO) in both the placenta and fetal brain at G29 (24 h after treatment). This endotoxin-mediated IDO induction was also associated with intense microglial activation, an increase in interferon gamma expression, and increases in kynurenine and the kynurenine pathway metabolites kynurenine acid and quinolinic acid, as well as a significant decrease in 5-hydroxyindole acetic acid (a precursor of serotonin) levels in the periventricular region of the fetal brain. These results indicate that maternal inflammation shunts tryptophan metabolism away from the serotonin to the kynurenine pathway, which may lead to excitotoxic injury along with impaired development of serotonin-mediated thalamocortical fibers in the newborn brain. These findings provide new targets for prevention and treatment of maternal inflammation-induced fetal and neonatal brain injury leading to neurodevelopmental disorders such as cerebral palsy and autism.

Dr. Sujatha Kannan, Department of Anesthesiology and Critical Care Medicine, Johns Hopkins University, Bloomberg Children's Center 6318D, 1800 Orleans Street, Baltimore, MD 21287 (USA), skannan3@jhmi.edu.

Keywords

Maternal infection; Cerebral palsy; Microglia; Tryptophan; Kynurenine pathway; Serotonin; Autism

Introduction

Maternal infection and inflammation have been implicated in white matter injury and periventricular leuko-malacia, and can lead to disorders such as cerebral palsy and is implicated in autism spectrum disorders [1–4]. Previous investigations by our group have shown that maternal intrauterine administration of noninfectious endotoxin lipopolysaccharide (LPS) on gestational day 28 (G28) results in motor deficits in the newborn rabbit (G31). Prenatal LPS treatment was also associated with activated microglia and astrocytes in the neonatal brain [5–8], increased proinflammatory cytokine levels and degeneration and abnormal arborization of the thalamic and cortical neurons [6, 9]. Studies by other groups have demonstrated increased tryptophan (TRP) metabolism by the kynurenine (KYN) pathway in the placenta in women with intrauterine infections [10] and in activated human microglia in culture [11], and may be related to the risk for autism spectrum disorders associated with prenatal infection [12].

TRP is an essential amino acid that can be metabolized along 2 metabolic pathways: methoxyindoles and KYNs [13]. Metabolism of TRP along the methoxyindole route results in the formation of 5-hydroxytryptamine (5-HT/ serotonin) and 5-methoxy-N-acetyltryptamine (melatonin) [14], The KYN pathway (Fig. 1) is a major degradative metabolic route for TRP, and a key regulator of the immune response. TRP is converted into KYN predominantly through 2 rate-limiting enzymes: indoleamine 2,3-dioxygenase (IDO), which is expressed in a number of cell types in the brain including astrocytes, microglia, microvascular endothelial cells, and macrophages [15] and also has roles in systemic inflammatory immune responses, and tryptophan 2,3-dioxygenase (TDO), which is also expressed in the brain [16–18], but is primarily responsible for systemic degradation of TRP into the cellular cofactor NAD+ in tissues such as the liver and kidney [19]. Unlike TDO, IDO expression is upregulated by interferon gamma (IFN-γ) [20] and proinflammatory cytokines [21–23], and is therefore highly induced during a myriad of inflammatory insults including bacterial and viral infections [24], KYN, a pivotal metabolite in the pathway, can in turn be metabolized via 2 distinct pathways: the neuroprotective kynurenic acid (KYNA) branch via the enzyme KYN amino transferase (KAT), and the neurotoxic branch leading to the production of 3-hydroxy-L-KYN (3-HK) and quinolinic acid (QUIN) via KYN monooxygenase (KMO) [25].

KYN pathway metabolism has been evaluated in the presence and absence of immune activation in patients [10, 26], nonhuman primates [27, 28], guinea pigs [29], mice [30], and rats [31]. Most recently, inflammation-induced activation of IDO in the brains of SIV-infected pigtailed macaques coincided with depletion of TRP in the CSF, increased levels of KYN and its downstream metabolites in the brain and CSF, a significant reduction in striatal serotonin levels, and an encephalitic pathology [28]. Additionally, intracerebroventricular

administration of LPS in mice triggered depressive-like symptoms that were linked to induction of the KYN pathway in the brain [32], suggesting KYN pathway involvement in a number of psychological and psychiatric disorders involving the TRP/serotonin axis [33]. Our previous study likewise demonstrated that maternal inflammation induced with endotoxin decreased cortical serotonin in neonatal rabbits in a model of cerebral palsy [34]. Serotonin functions as a neurotransmitter and a substrate for melatonin synthesis in the central nervous system. Serotonin also plays an important role in the developing brain, influencing neurogenesis, neuronal migration, and synaptogenesis [35], and regulates differentiation of its target cells in the developing brain [36]. Deficient production of serotonin contributes to the delayed neuronal cortical development [37, 38], disruption of thalamocortical afferents [39], disturbances in circadian rhythm and sleep, and the pathogenesis of depression [40]. In this study, we in-vestigated the effects of in utero endotoxin exposure on the KYN pathway by measuring the expression of IFN-γ, IDO, KAT, and KMO, as well as the quantification of TRP and its major metabolites in the placenta and fetal brain. A better understanding of the role of maternal inflammation-induced alterations in TRP metabolism is crucial for the development of therapeutic strategies targeted toward manipulating the KYN pathway in preventing fetal and neonatal brain injury.

Materials and Methods

Animal Model

All animal procedures were approved by the Institutional Animal Care and Use Committee at Johns Hopkins University. Timedpregnant New Zealand white rabbits were purchased from Robinson Services Inc. (Mocksville, NC, USA). After 1 week of acclimation, rabbits were randomly divided into control (n = 10) and endotoxin (n = 10) groups. The average weight of the pregnant rabbits was 4.7 kg. Pregnant rabbits in the endotoxin group underwent laparotomy under general anesthesia at G28, and ~8,000 EU of LPS (*Escherichia coli* serotype O127:B8; Sigma Aldrich, St. Louis, MO, USA) was injected along the wall of the uterus as previously described [8]. The control group did not receive any treatment except for intravenous fluids. One day after surgery (G29), dams were euthanized with an overdose of pentobarbital (120 mg/ kg) intravenously. For each dam, fetuses were rapidly removed from the uterus, and fetal brains and placentae were harvested. For region-specific analysis, the brain was cut in the coronal plane using a brain block and the periventricular region (PVR), including the corpus callosum, corona radiata, lateral ventricles, and part of the dorsal hippocampus were dissected. The fetal brains were processed differently for each of the measures and littermates were taken for the different studies.

Real-Time PCR

Total RNA from the fetal brain PVR or the placenta (50–100 mg fresh tissue) was extracted using TRIzol (Life Technologies, Grand Island, NY, USA) according to the manufacturer's instructions (n = 6–12 kits per each group). RNA samples were quantified using the Nanodrop ND-1000 Spectrophotometer. The single-stranded complementary DNA (cDNA) was first reverse transcribed from the total RNA samples using the High Capacity cDNA Reverse Transcription Kit with RNase inhibitor (Life Technologies, USA). Real-time PCR was performed with SYBR Green PCR Master Mix (Life Technology, USA) using Fast 7500

Realtime PCR systems (Life Technologies, USA). Amplification conditions included 30 min at 48° C, 10 min at 95°C, 40 cycles at 95°C for 15 s, and60°C for 1 min. The samples were analyzed for mRNA expression of IFN-γ, IDOl, KMO, and KAT-2 (responsible for the KYNA production in the brain), using primers designed for rabbits. A list of primers and their specifications are detailed in Table 1. Primers were custom designed and ordered from Integrated DNA Technology. The comparative C_t method was used to assess differential gene expression between the control and endotoxin groups at different time points. First, gene expression levels for each sample were normalized to the expression level of the housekeeping gene encoding glyceraldehyde 3-phosphate dehydrogenase (GAPDH) within a given sample (ΔCT); the difference between the endotoxin and control groups were used to determine the ΔΔCT. $2^{-\Delta\Delta CT}$ gave the relative fold increase in gene expression of the control and endotoxin animals.

Immnohistochemistry

G29 rabbit kits were anesthetized and intracardially perfused with saline followed by 10% formalin and then postfixed for 24 h. Brains were then cryoprotected with sucrose and 30-μm cryostat sections were mounted onto poly-L-lysine-coated slides (Sigma Aldrich, USA). The sections were blocked with 3% donkey serum followed by incubation with goat polyclonal anti-Ibal primary antibody (1:250; Abeam, Cambridge, MA, USA) overnight at 4°C. After washing, sections were incubated with Alexa Fluor® 488 donkey anti-goat IgG (H+L) secondary antibody (1:250; Life Technologies, USA) for 2 h at room temperature, and then incubated with DAPI (1:1,000; Invitrogen) for 15 min. The slides were washed, dried, and cover slipped with mounting medium (Dako, Carpinteria, CA, USA). Colocalization of GFAP/IDO was done by incubating the sections overnight at 4°C with chicken anti-GFAP (1:250; Abeam, USA)/mouse anti-IDO (1:200; GeneTex, USA). Colocalization of IBA1/IDO was done by incubating the sections overnight at 4°C with goat anti-IBAl (1:250; Abeam, USA) and mouse anti-IDO (1:200; GeneTex, USA). Sections were subsequently washed and incubated with fluorescent secondary antibodies (1:250; Life Technologies, USA) for 2 h at room temperature. Next, the sections were incubated with DAPI (1:1,000; Invi-trogen) for 15 min. After wash, the slides were dried and cover slipped with mounting medium (Dako, USA). Confocal images were acquired with Zeiss ZEN LSM 710 (Zeiss, USA) and processed with ZEN software (version 10.0).

Cell Counts

All slides and images were coded and the analysis was performed with the personnel blinded to the experimental groups. Confocal images (x63; 4–6 images/animal) were randomly acquired from corpus callosum using Zeiss ZEN LSM 710 (Zeiss, USA). The confocal images were exported into individual channels using ZEN software (version 10.0). The $IBA1^+$ (green), IDO^+ (red), and IBA^+/IDO^+ (merged) cells were counted and averaged to the area of the region of interest.

Gas Chromatography-Mass Spectrometry

Dissected PVR brain tissue and placental tissue were weighed and diluted 1/20 (weight/volume) with ice-cold 0.1% ascorbic acid and sonicated 3 times at 30% amplitude for 3 s on ice. On ice, brain homogenates (50 μL) were spiked with 50 μL of a heavy standard solution

containing 1 μM [$^2H_5$] TRP (CDN Isotopes, Canada), 5 μM [$^2H1_6$] KYN (custom synthesis from Sigma Aldrich Isotec), and 0.2 μM [$^2H_3$] QUIN (custom synthesis from Synfine, Canada). Samples were spiked with 50 μL of−20°C acetone and centrifuged at 20,000 *g* for 5 min. The supernatants (120 μL) were transferred to microcentrifuge tubes, spiked with 50 μL of a 2:5 ratio methanolxhloroform, and centrifuged at 20,000 *g* for 10 min. The aqueous layers (80 μL) were transferred to glass vials and evaporated to dryness. Samples were derivatized with 120 μL of 2,2,3,3-pentafluoro-l-propanol (Sigma) and 135 μL of pentafluoropropionic anhydride (Sigma) by heating at 75”C for 30 min. Derivatized samples were evaporated to dryness and stored at−80°C. GC/MS/MS conditions and multiple reaction monitoring transitions were as previously described [41]. Deidentified samples were injected in a randomized order at least twice. Data were analyzed with Agilent MassHunter software, Build B.04. Peak areas for each compound were normalized to their heavy standards. These values were then fit to the matrix-spiked light standard curve for each compound based on the standard addition method. No heavy standard was spiked in for 3HK, which was instead normalized to heavy KYN because of their similar properties.

High-Performance Liquid Chromatography

The placenta or PVR tissues (~200 mg) were homogenized in 1 mL of deionized water, centrifuged at 15,000 rpm for 10 min, and then 1 mL of the supernatant was collected and vortexed with 3 mL of chloroform to remove fatty acids and lipids. Obtained mixtures were centrifuged at 4,000 rpm for 10 min. The aqueous fraction (0.8 mL) was mixed with acetonitrile (3 mL) for protein precipitation and left on ice for 30 min for their coagulation, followed by centrifugation at 4,000 rpm for 10 min at 4°C. The supernatant was divided into 2 aliquots of 1.6 mL each and evaporated under vacuum. For high-performance liquid chromatography (HPLC) analysis, residues were dissolved in 1 mL of deionized water and 3 injections of 200 μL for each sample were performed. All processed samples were analyzed using a Waters 1525 binary HPLC separation module (Waters Corp., Milford, MA, USA), equipped with an in-line degasser AF, a 717 Plus autosampler (kept at 4°C), a 2998 PDA detector, and a 2475 multiwavelength fluorescence detector, controlled by Empower software. Isocratic separations were run on TSK-Gel ODS-80 Ts (250 × 4.6 mm i.d., 5 μm) and TSK-Gel guard columns with 0.1% acetic acid in H_2OACN (90:10 v/v) at a flow rate of 0.6 mL/min. Elution was simultaneously monitored by a PDA detector (collecting UV-Vis spectra from 190 to 800 nm, which can provide chromatograms at the desired wavelength in this range) as well as a fluorescence detector having 3 channels set as follows: channel 1 - excitation at 297 nm and emission at 344 nm for detection of TRP and 5-hydroxyindole acetic acid (5HIAA); channel 2 - excitation at 330 nm and emission at 390 nm for detection of KYNA; and channel 3 - excitation at 364 nm and emission at 480 nm for detection of KYN. The calibration curves and the limits of detection for each analyte were obtained by injecting various amounts of the analytes (ranging from 1 pg to 1 μg) into the HPLC, and used as reference calibration curves for their quantification in the placental samples and in PVR brain tissue obtained from fetal rabbits (gestation day 29). Data from the HPLC measurements are expressed as ratios of the metabolite to its substrate for KYNA/KYN and 5HIAA/TRP.

Statistical Analysis

The RNA expression data and metabolite values were normalized by log transformation prior to statistical analysis. The log transformation helped to reduce the variability in the data and the effect of outliers on the final analysis [42]. Kits were nested within litters for the analysis. Generalized estimating equations with an exchangeable correlation structure were used to investigate the difference between log-transformed RNA expression in treatment (endotoxin) versus control. We used generalized estimating equations because it takes into account independence of observations within litters. The analyses were performed using R version 3.2.2 (R foundation for Statistical Computing, Vienna, Austria). Statistical significance was set as $p < 0.05$, and all tests were 2-sided. Data is expressed as medians and interquartile ranges in the graphs. GraphPad prism was used to generate the graphs.

Results

Maternal Inflammation-Induced Changes in Microglial Morphology

The extent of microglial activation was assessed by immunohistochemistry using the specific microglial marker, Iba1. In the control group, the microglial cells were ramified with multiple branches, whereas the microglial cells in the endotoxin group had hypertrophied soma and shortened branches. In addition, a subset of the microglial cells in the endotoxin group had an amoeboid shape, and no ramifications could be detected on the cells (Fig. 2). This change in morphology (associated with activation) was noted extensively in the regions of the corpus callosum, the angle of the lateral ventricles, and the internai capsule in the endotoxin kits (Fig. 2), and was similar to what had been observed previously in this model [8].

Maternal Inflammation Upregulates the KYN Pathway in the Fetal Brain

We measured IDO1, KAT-2, KMO, and IFN-γ mRNA expression in G29 brains and placenta from control and endotoxin-treated groups. The range of the variability in the log-transformed mRNA expression data was 0.0001–1.9. There was a 6-fold increase in mRNA expression of IFN-γ in the PVR of the fetal brain in endotoxin kits when compared to age-matched controls ($p = 0.001$). This was associated with a 5-fold increase in expression of IDO1 and a 2-fold increase in KMO in the endotoxin kits ($p = 0.008$ and $p = 0.01$, respectively, when compared to controls). There was no significant change in the expression of KAT-2 ($p = 0.79$) (Fig. 3a-d). In addition, we also measured TDO mRNA expression (control: 0.70 [0.23, 5.08] vs. endotoxin 0.59 [0.11, 11.25]; $p = 0.08$) and TPH (control 0.56 [0.41, 0.87] vs. endotoxin 2.92 [1.19, 5.57]; $p = 0.08$), and there was no significant difference.

To correlate this with the functional activity of the enzymes, the major metabolites of the KYN pathway were measured in the fetal brains of control and endotoxin-exposed littermates using GCMS and HPLC (see Methods). KYN levels were significantly elevated in the PVR of G29 endotoxin kits when compared to controls ($p < 0.01$). However, there was no significant difference in TRP levels in the PVR between the groups, indicating that this is related to the upregulation of IDO in this region (Fig. 3e, f). This increase in KYN was associated with an increase in the QUIN levels in the PVR of endotoxin kits ($p < 0.001$)

(Fig. 3g). A significant increase in the neuroprotective metabolite KYNA was noted in the endotoxin-exposed G29 kits (Fig. 3h). While there was a significant difference in KYNA, there was no difference in KAT-2 mRNA expression, the enzyme which metabolizes KYN to KYNA. Increased KYNA may be related to increased KYN precursor for KAT-2 or due to increased expression of the KAT-2 protein (not measured). A significant decrease in the serotonin metabolite 5HIAA was noted in the G29 kits (Fig. 3i), indicating decreased conversion of TRP to serotonin due to shunting of TRP along the KYN pathway in the fetal brain exposed to maternal intrauterine inflammation. This is in accordance with our previous studies where decreased serotonin was seen in the cortex and PVR of newborn rabbit kits exposed to maternal inflammation.

Maternal Intrauterine Inflammation Leads to Dysregulated TRP-KYN Metabolism in the Placenta

In the placenta there was a significant increase in placental IDOl mRNA expression (~3-fold higher expression, $p < 0.001$) and KMO expression (21-fold higher, $p < 0.001$) in the endotoxin-treated dams compared to controls. No significant change in placental expression of IFN-γ ($p = 0.09$) or KAT2 ($p = 0.16$) mRNA was noted between the groups (Fig. 4a-d). Although there was a decrease in both the TRP and KYN levels in the placenta of endotoxin kits when compared to the controls (Fig. 4e, f), a significant increase was noted in the KYN to TRP ratio (Fig. 4h), indicating that most of the TRP was being converted to KYN in the placenta of endotoxin-exposed rabbits as confirmed by the increased expression of IDO1 mRNA. In spite of a decrease in the KYN level, no significant difference was noted in QUIN levels between the endotoxin and control placenta (Fig. 4g). This along with the increased expression of KMO indicates that more of the KYN in the endotoxin kits is converted to QUIN when compared to controls.

IDO Is Colocalized with Astrocytes and Microglia in the PVR in Control and Endotoxin Kits

Previously, IDO has been shown to be expressed in both astrocytes and microglia cells [43,44]. We costained GFAP/IDO and IBA1/IDO and analyzed the colocalization of IDO with astrocytes and/or microglia on G29 (control = 3 kits, from 1 litter; endotoxin = 5 kits, from 3 litters). We found that IDO was colocalized with astrocytes (fig. 5a, b) and microglia (Fig. 5c, d) in both control and endotoxin kits on G29. The IDO antibody mainly stained the soma and proximal processes of the astrocytes and microglia. However, the overall IDO staining was greater in the activated microglial cells in the endotoxin kits due to the increased soma size (fig. 5c, d). We further quantified the number of $IBA1^+$ (microglial marker), IDO^+, and IBA^+/IDO^+ cells in the corpus callosum in both control and endotoxin-exposed kits. We found that the IBAD (control 365 ± 22/mm^2 vs. endotoxin 1,033 ± 118/mm^2, $p < 0.0001$), IDO^+ (control 334 ± 22/mm^2 vs. endotoxin 1,026 ± 114/mm^2, $p < 0.0001$), and IBA^+/IDO^+ (control 334 ± 22/mm^2 vs. endotoxin 1,013 ± 117/mm^2, $p < 0.0001$) cells were significantly increased in endotoxin-exposed kits. These results are consistent with the increased IDO mRNA expression and increased functional activity of the enzyme as evidenced by the KYN levels in the PVR. This indicates that the KYN pathway activation in the endotoxin-exposed brains is primarily by the microglia.

Discussion

In this study, we used a rabbit model of maternal uterine inflammation to investigate dysregulation of TRP metabolism in the placenta and fetal brain. We administrated LPS (8,000 EU of ultrapure endotoxin of 0127:B8strain of *E. coli*) into the wall of the uterus at G28 (late term), which mimics the most common human scenario of subclinical chorioamnionitis (close to full term), where the dam is relatively unaffected but the newborn rabbits are affected. The ultrapure form of LPS was used since this has <1% contamination with protein or RNA, in or-der to minimize off target effects. The same batch and lot numbers were maintained between experiments to minimize variability. The endotoxin dose (8,000 EU) used in our study is equivalent to ~20 μg/kg of *E. coli* endotoxin. We have previously demonstrated that this dose of LPS at G28 (late term) leads to ~70% survival at birth, without maternal mortality, and rabbit kits exposed to maternal inflammation showed motor deficits and hypertonia, a behavioral phenotype similar to that seen in children with spastic cerebral palsy [8]. In addition, our previous studies demonstrated that there was robust microglial activation in the brain PVR that up to postnatal day 8, hypomy-elination in the white matter areas [6–8], neuronal injury in anterior thalamus and retrosplenial cortical regions [9], decreased serotonin staining in thalamocortical fibers in the parietal somatosensory cortex [34], and increased glutamate excitotoxicity [45], consistent with histological findings reported in postmortem brain of human neonates with periventricular leukomalacia [46]. Similar methods have been used in mouse models, in which intrauterine infusion of LPS (250 μg in 100 μL) induced preterm birth and decreased microtubule-associated protein 2 staining, and decreased the number of dendrites in the mouse fetal brain [47].

Variability between models and studies evaluating effects of prenatal LPS exposure have been described, which may be due to variations in the LPS make, lot, batch, purity, mode of administration, and species specific response to the LPS [48]. Although the LPS dose, route of administration and time of gestation might be different, the majority of studies demonstrate that the prenatal neuroinflammation induced by LPS results in abnormal brain development and behavioral deficits. For example, LPS (200 ng, intravenous bolus infusion) has been administered to preterm fetal sheep (70% gestation) prior to myelination onset, and leads to impairment in both white matter and cortical development [49]. LPS administration (300 μg, intraperitoneally) at 70% gestation to the pregnant guinea pigs induces cell death in the brain of neonate offspring [50]. In rodent models, maternal exposure to LPS (100 μg/kg, intraperitoneally) at G15/16 (midterm) induced social behavior changes in neonate rats [51], while maternal exposure to LPS (300 μg/kg, intraperitoneally) at G19/20 (later term) leads to transient motor dysfunction in neonatal rats [52]. In a rat model, maternal exposure to LPS (100 μg/kg q12 h intraperitoneally from E17 to birth) followed by HI after birth led to motor deficits involving both spontaneous and forced motor activities along with extensive bilateral cortical and subcortical lesions of diffuse motor networks mimicking deficits in human preterm infants [53].

Using our rabbit intrauterine LPS inflammation model, we demonstrate here that maternal inflammation at G28 significantly increased IFN-γ and IDO1 mRNA in the PVR of the fetal brain following endotoxin exposure at G29 (1 day after injury). The induction in IDO1

mRNA expression was associated with increases in levels of KYN, KYNA, and QUIN in the brain of endotoxin-exposed kits. Conversely, there was a significant decrease in the ratio of the serotonin metabolite 5HIAA to TRP in the brains of the endotoxin-exposed kits, suggesting the shunting of TRP metabolism from the serotonin pathway to formation of the KYN pathway metabolites. In the brain, this upregulation of the KYN pathway appears to be driven by microglial activation in the PVR of the fetal brain as evidenced by changes in microglial morphology determined by Iba1 staining and increased IDO staining that colocalized with the “activated microglia.” Activated microglial cells are known to accelerate conversion of TRP into QUIN [11, 54]. which is consistent with increased QUIN levels in the PVR in our study.

Maternal infection-induced immune responses in offspring, such as microglial activation and cytokine/chemokine release, are associated with TRP pathway dysfunction and development of perinatal brain injury [34]. Proinflammatory cytokines, such as IFN-γ [55–57], TNF-α [58]. IL-1, IL-12, IL-18, and PGE2 [59, 60] can transcriptionally induce IDO in a variety of immune cells. Previous studies have shown that IDO is upregulated in activated microglia in the mouse cerebellum during acute viral encephalitis [61]. The increased IDO in our study might be due to marked microglial activation and increased proinflammatory cytokines, such as IFN-γ, TNF-α, and IL-1β, in the PVR region, which are consistent with these previous studies [20, 24, 62].

IDO is the rate-limiting enzyme for the conversion of TRP to KYN; therefore, an increased IDO level could shift the balance of TRP metabolism toward formation of KYN [63]. Serotonin plays an important role in the formation of thalamocortical afferents, neuronal development, and maturation [for recent review, see 64], and is associated with abnormal neuronal architecture in newborn rabbits [9]. Recent studies indicate that fetal brain hypoxia-ischemia induces tetrahydrobiopterin (BH4) insufficiency, and tetrahydrobiopterin treatment can prevent hypertonia in hypoxic fetal brain in the newborns [65, 66]. BH4 is a natural pterin and an essential cofactor for aromatic amino acid hydroxylases, such as tyrosine hydroxylase and TRP hydroxylase [67]. TRP hydroxylase is the rate-limiting enzyme in the biosynthesis of serotonin [67]. Therefore, BH4 deficiency may also decrease serotonin levels. It is possible that an added BH4 deficiency along with the IDO upregulation may result in a more severe serotonin deficiency in the developing brain.

KYN can be further metabolized by either the KYNA pathway that leads to formation of KYNA, an NMDA antagonist [68], or the nicotinamide adenine dinucleotide (NAD) pathway that leads to formation of the NMDA agonist QUIN and free radical generators (3-hydroxy-KYN and 3-hydroxyanthranilic acid) [69]. It has been shown that KYNA in physiological concentrations exerts a neu-romodulatory effect, while elevated concentrations of KYNA under pathological conditions can inhibit NMDA receptor hyperactivation and ameliorate glutamate excitotoxicity [70]. QUIN, on the other hand, is a specific competitive agonist of the NR2A and NR2B NMDA receptor subtypes. Under pathological conditions, elevated QUIN can activate NMDA receptors, provoke lipid peroxidation, potentiate oxidative stress [29], and induce release of cytokines such as IFN-γ, IL-1β, and TNF-α from astrocytes [71]. These proinflammatory cytokines in turn will further upregulate the expression of IDO, thereby increasing TRP metabolism to KYN. Proinflammatory cytokines

also activate KMO, which converts KYN into 3-HK and further shifts the KYN pathway towards the neurotoxic 3-HK/QUIN pathway instead of KYNA. We did in fact find that elevations in IFN-γ were associated with elevations in KMO in the PVR of endotoxin kits and in the placenta, as well as an overall increase in QUIN levels in both the endotoxin kits and placentas compared to controls. However, 3HK levels were unchanged in the tissues and were close to the limit of detection, which may reflect the extremely labile nature of 3HK and its rapid turnover into downstream metabolites. Importantly, the significantly increased formation of QUIN that we observed could result in NMDA-mediated excitotoxicity [72–74], and might contribute to the motor deficits and higher mortality seen in kits exposed to endotoxin [8]. Studies show that QUIN increases neuronal glutamate release, decreases astrocytes glutamate uptake, and inhibits astroglial glutamine synthetase, potentiating glutamate toxicity [71, 75, 76]. Moreover, QUIN promotes ROS generation [77–79], increases nitric oxide production [80] and phosphorylation of cellular structural proteins and tau [81, 82], leading to dysregulation of astroglial functions [83]. Therefore, QUIN can be used as a biomarker that indicates activation of KYN pathway metabolism.

We also found that the KYNA levels were significantly increased in the fetal brain. The increased KYNA level in the endotoxin kits may be a compensatory, protective response toward inflammation-induced excitotoxicity. We have previously shown that the NMDA receptors NR2A and NR2B are upregulated in the fetal brain exposed to endotoxin [45]. This is associated with increased glutamate levels in the fetal brain [45] that can work synergis-tically with QUIN in promoting excitotoxicity. However, studies also show that persistent and chronic elevations of KYNA can induce excessive NMDA receptor and α7 nicotinic acetylcholine receptor (a7nAChR) antagonism, which has been implicated in the pathogenesis of psychiatric disorders, such as schizophrenia [84, 85]. In this case, the elevated KYNA level can be both beneficial and detrimental, which needs to be further investigated over time in our model.

Studies show that placental 5-HT synthesis from maternal TRP precursor contributes to fetal 5-HT during crucial periods in utero in mice [86–89]. The time during which 5-HT synthesized in the placenta contributes to brain 5-HT in the mouse corresponds to the first trimester and early second trimester in humans [87]. In mice, the 5-HT source for the forebrain is primarily exogenous from the placenta till late gestation, after which serotonin is produced endogenously in the fetal and newborn brain [87]. Our results demonstrating upregulation of IDO in the placenta after maternal inflammation is consistent with other previous studies [10, 90, 91], A recent study demonstrated a transient increase in placental TRP and increased 5-HT levels in the forebrain of fetal mice exposed to a low level poly-I:C-induced maternal inflammation during midgestation that was not associated with increased cytokines in the fetal brain [91]. However, in our study we found that placental TRP levels were significantly lower in the rabbits exposed to *E. coli* endotoxin near term, when compared to age-matched controls. This may be due to decreased transport of TRP because of competition of other amino acids at the AA transporter in the placenta in the presence of inflammation [92]. Increased shunting of TRP to the fetus may explain the preservation of the TRP levels in the fetal brains even in the endotoxin kits. In our study we showed a significant decrease in the level of the serotonin metabolite 5HIAA in the fetal PVR, in spite of no differences in TRP levels in the brain between control and endotoxin

kits, indicating that the up-regulation of the KYN pathway and KYN metabolites in the brain occurs independently from that in the placenta. We also measured the mRNA expression of TPH, and we found that its expression is similar to what we have previously noted in postnatal day 1 rabbits where there was no difference in TPH 1/2 detected between the endotoxin and control kits [34], The decrease in serotonin metabolite and serotonin in the fetal and newborn brain (present study and [34]) appears to be primarily related to the robust neuroinflammation and microglial activation, induced by proinflammatory cytokines such as IFN-γ, in the PVR of the fetal and newborn brain that shunts TRP metabolism towards KYN pathway in this model. This is also in accordance with other studies involving patients with neuroinflammatory disorders, where the KYN/TRP ratio is elevated even when the TRP levels may be low, indicating upregulation of the KYN pathway [33, 93]. A limitation of this study is that the extent of microglial activation could not be correlated directly with the changes in KYN metabolites in the same brain. This is because the fetal brain is small, and due to differences in methods used to process the tissue, the same tissue could not be used for different measures. However, we show an increase in the IDO-positive microglia in the fetal brains exposed to maternal inflammation. This indicates that maternal endotoxin exposure leads to upregulation of the KYN pathway in the fetal microglia.

Understanding the effect of abnormal TRP metabolism in the perinatal period will facilitate the design of specific therapies targeted towards this pathway in the fetus and neonate. The IDO levels were significantly elevated in both the placenta and fetal brains at G29 following endotoxin treatment; hence, therapies that inhibit IDO might be beneficial in the early postnatal period following exposure to intrauterine inflammation. Because inhibition of IDO during pregnancy leads to allogeneic rejection of the fetus [94, 95], targeting this enzyme in the prenatal period is not a viable therapeutic option. However, postnatal IDO inhibition may be feasible, especially if IDO expression continues to be persistently elevated in neonates due to ongoing neuroinflammation and microglial activation. Meanwhile, the expression of KMO was higher in the G29 fetal brains and the placentas in the endotoxin kits, which suggests that a prenatal treatment with a KMO inhibitor that can cross the placenta could potentially be helpful.

Conclusion

In this study, we demonstrate that the maternal intrauterine inflammation induced by a bacterial endotoxin induces the dysregulation of TRP metabolism, which might be responsible for impaired thalamocortical development in the fetus and newborn. Altered KYN pathway metabolites may promote neurotoxicity while decreased 5-HT may lead to developmental changes related to altered developmental regulation. These findings can facilitate the design of therapeutic strategies targeted towards manipulating the KYN pathway both prenatally and postnatally, and for the prevention of fetal and neonatal brain injury and altered developmental regulation.

Acknowledgements

This project is supported by a T-32 (5T32GM075774) grant awarded to Dr. Monica Williams and a NIH R01 (R01HD069562) grant awarded to Dr. Sujatha Kannan.

References

1. Yoon BH, Park CW, Chaiworapongsa T: Intrauterine infection and the development of cerebral palsy. BJOG 2003; 110(suppl 20):124– 127. [PubMed: 12763129]
2. Bashiri A, Burstein E, Mazor M: Cerebral palsy and fetal inflammatory response syndrome: a review. J Perinat Med 2006;34:5–12. [PubMed: 16489880]
3. Burd I, Balakrishnan B, Kannan S: Models of fetal brain injury, intrauterine inflammation, and preterm birth. Am J Reprod Immunol 2012;67:287–294. [PubMed: 22380481]
4. Langridge AT, et al.: Maternal conditions and perinatal characteristics associated with autism spectrum disorder and intellectual disability. PLoS One 2013;8:e50963. [PubMed: 23308096]
5. Kannan S, et al.: Microglial activation in perinatal rabbit brain induced by intrauterine inflammation: detection with ^{11}C-(R)-PK11195 and small-animal PET. J Nucl Med 2007;48: 946–954. [PubMed: 17504871]
6. Kannan S, et al.: Dendrimer-based postnatal therapy for neuroinflammation and cerebral palsy in a rabbit model. Sci Transl Med 2012; 4:130ra46.
7. Kannan S, et al.: Magnitude of [^{11}C]PK11195 binding is related to severity of motor deficits in a rabbit model of cerebral palsy induced by intrauterine endotoxin exposure. Dev Neuro-sci 2011;33:231–240.
8. Saadani-Makki F, et al.: Intrauterine administration of endotoxin leads to motor deficits in a rabbit model: a link between prenatal infection and cerebral palsy. Am J Obstet Gynecol 2008; 199: 651e1–7. [PubMed: 18845289]
9. Balakrishnan B, et al.: Maternal endotoxin exposure results in abnormal neuronal architecture in the newborn rabbit. Dev Neurosci 2013;35:396–405. [PubMed: 23988854]
10. Manuelpillai U, et al.: Identification of kyn-urenine pathway enzyme mRNAs and metabolites in human placenta: up-regulation by inflammatory stimuli and with clinical infection. Am J obstet Gynecol 2005;192:280–288. [PubMed: 15672037]
11. Heyes MP, et al.: Human microglia convert l-tryptophan into the neurotoxin quinolinic acid. Biochem J 1996;320:595–597. [PubMed: 8973572]
12. Schwartz CE: Aberrant tryptophan metabolism: the unifying biochemical basis for autism spectrum disorders? Biomark Med 2014; 8: 313–315. [PubMed: 24712420]
13. Gal EM, Sherman AD: L-kynurenine: its synthesis and possible regulatory function in brain. Neurochem Res 1980;5:223–239. [PubMed: 6154900]
14. Kopin IJ, et al.: The fate of melatonin in animals. J Biol Chem 1961;236:3072–3075. [PubMed: 14458327]
15. Hayaishi O: Properties and function of in-doleamine 2,3-dioxygenase. J Biochem 1976; 79: 13P–21P.
16. Guillemin GJ, et al.: Characterization of the kynurenine pathway in human neurons. J Neurosci 2007;27:12884–12892. [PubMed: 18032661]
17. Miller CL, et al.: Expression of the kynurenine pathway enzyme tryptophan 2,3-dioxygenase is increased in the frontal cortex of individuals with schizophrenia. Neurobiol Dis 2004; 15: 618–629. [PubMed: 15056470]
18. Haber R, et al.: Identification of tryptophan 2,3-dioxygenase RNA in rodent brain. J Neu-rochem 1993;60:1159–1162.
19. Lob S, et al.: Inhibitors of indoleamine-2,3-di-oxygenase for cancer therapy: can we see the wood for the trees? Nat Rev Cancer 2009; 9: 445–452. [PubMed: 19461669]
20. Chen S, et al.: Natural inhibitors of indole-amine 3,5-dioxygenase induced by interferon-gamma in human neural stem cells. Biochem Biophys Res Commun 2012;429:117–123. [PubMed: 23063682]
21. Yang JM, et al.: Acetylsalicylic acid enhances the anti-inflammatory effect of fluoxetine through inhibition of NF-KB, p38-MAPK and ERK1/2 activation in lipopolysaccharide-induced BV-2 microglia cells. Neuroscience 2014;275:296–304. [PubMed: 24952332]

22. Liu WL, et al.: Epstein-Barr virus infection induces indoleamine 2,3-dioxygenase expression in human monocyte-derived macrophages through p38/mitogen-activated protein kinase and NF-KB pathways: impairment in T cell functions. J Virol 2014;88:6660–6671. [PubMed: 24696473]
23. Yu J, et al.: Noncanonical NF-κB activation mediates STAT3-stimulated IDO upregula-tion in myeloid-derived suppressor cells in breast cancer. J Immunol 2014; 193:2574–2586. [PubMed: 25063873]
24. Yadav MC, et al.: IFN-gamma-induced IDO and WRS expression in microglia is differentially regulated by IL-4. Glia 2007; 55: 1385–1396. [PubMed: 17661345]
25. Robotka H, et al.: Neuroprotection achieved in the ischaemic rat cortex with L-kynurenine sulphate. Life Sci 2008;82:915–919. [PubMed: 18387638]
26. Yan EB, et al.: Activation of the kynurenine pathway and increased production of the ex-citotoxin quinolinic acid following traumatic brain injury in humans. J Neuroinflammation 2015; 12:110. [PubMed: 26025142]
27. Heyes MP, Lackner A: Increased cerebrospinal fluid quinolinic acid, kynurenic acid, and L-kynurenine in acute septicemia. J Neuro-chem 1990;55:338–341.
28. Drewes JL, et al.: Quinolinic acid/tryptophan ratios predict neurological disease in SIV-in-fected macaques and remain elevated in the brain under cART. J Neurovirol 2015;21:449–463. [PubMed: 25776527]
29. Blight AR, Saito K, Heyes MP: Increased levels of the excitotoxin quinolinic acid in spinal cord following contusion injury. Brain Res 1993;632:314–316. [PubMed: 8149236]
30. Saito K, Markey SP, Heyes MP: Effects of immune activation on quinolinic acid and neuroactive kynurenines in the mouse. Neuroscience 1992;51:25–39. [PubMed: 1465184]
31. Leib SL, et al.: Neuroprotective effect of excitatory amino acid antagonist kynurenic acid in experimental bacterial meningitis. J Infect Dis 1996;173:166–171. [PubMed: 8537654]
32. Lawson MA, et al.: Intracerebroventricular administration of lipopolysaccharide induces indoleamine-2,3-dioxygenase-dependent depression-like behaviors. J Neuroinflammation 2013;10:87. [PubMed: 23866724]
33. Chiappelli J, et al.: Tryptophan metabolism and white matter integrity in schizophrenia. Neuropsychopharmacology 2016; 41:2587–2595. [PubMed: 27143602]
34. Kannan S, et al.: Decreased cortical serotonin in neonatal rabbits exposed to endotoxin in utero. J Cereb Blood Flow Metab 2011; 31 : 738–749. [PubMed: 20827261]
35. Lauder JM, Krebs H: Serotonin as a differentiation signal in early neurogenesis. Dev Neu-rosci 1978;1:15–30.
36. Lauder JM: Serotonin as a differentiation signal. Dev Neurosci 2016;38:239–240. [PubMed: 27701168]
37. Cases O, et al.: Lack of barrels in the somatosensory cortex of monoamine oxidase A-defi-cient mice: role of a serotonin excess during the critical period. Neuron 1996;16:297–307. [PubMed: 8789945]
38. Persico AM, et al.: Barrel pattern formation requires serotonin uptake by thalamocortical afferents, and not vesicular monoamine release. J Neurosci 2001;21:6862–6873. [PubMed: 11517274]
39. Blue ME, Erzurumlu RS, Jhaveri S: A comparison of pattern formation by thalamocortical and serotonergic afferents in the rat barrel field cortex. Cereb Cortex 1991;1:380–389. [PubMed: 1822748]
40. Nestler EJ, et al.: Neurobiology of depression. Neuron 2002;34:13–25. [PubMed: 11931738]
41. Notarangelo FM, et al.: Gas chromatography/ tandem mass spectrometry detection of extracellular kynurenine and related metabolites in normal and lesioned rat brain. Anal Biochem 2012;421:573–581. [PubMed: 22239963]
42. Gelman A, Hill J: Data Analysis Using Regression and Multilevel/Hierarchical Models Analytical Methods for Social Research. Cambridge, Cambridge University Press, 2007, vol xxii, p 625.
43. Guillemin GJ, et al.: Expression of indoleamine 2,3-dioxygenase and production of quinolinic acid by human microglia, astrocytes, and neurons. Glia 2005;49:15–23. [PubMed: 15390107]
44. Kwidzinski E, et al.: IDO (indolamine 2,3-dioxygenase) expression and function in the CNS. Adv Exp Med Biol 2003;527:113–118. [PubMed: 15206723]

45. Zhang Z, et al.: Maternal inflammation leads to impaired glutamate homeostasis and up-regulation of glutamate carboxypeptidase II in activated microglia in the fetal/newborn rabbit brain. Neurobiol Dis 2016;94:116–128. [PubMed: 27326668]
46. Haynes R, Reading R, Gale S: Household and neighbourhood risks for injury to 5–14 year old children. Soc Sci Med 2003; 57: 625–636. [PubMed: 12821011]
47. Burd I, et al.: Inflammation-induced preterm birth alters neuronal morphology in the mouse fetal brain. J Neurosci Res 2010;88: 1872–1881. [PubMed: 20155801]
48. Dean JM, et al.: A critical review of models of perinatal infection. Dev Neurosci 2015;37: 289–304. [PubMed: 25720344]
49. Dean JM, et al.: Delayed cortical impairment following lipopolysaccharide exposure in preterm fetal sheep. Ann Neurol 2011;70:846– 856. [PubMed: 22002627]
50. Harnett EL, Dickinson MA, Smith GN: Dose-dependent lipopolysaccharide-induced fetal brain injury in the guinea pig. Am J Obstet Gynecol 2007;197:179e1–7. [PubMed: 17689642]
51. Baharnoori M, Bhardwaj SK, Srivastava LK: Neonatal behavioral changes in rats with gestational exposure to lipopolysaccharide: a prenatal infection model for developmental neuropsychiatric disorders. Schizophr Bull 2012;38:444–456. [PubMed: 20805287]
52. Rousset CI, et al.: Maternal exposure to lipopolysaccharide leads to transient motor dysfunction in neonatal rats. Dev Neurosci 2013; 35:172–181. [PubMed: 23445561]
53. Girard S, et al.: Developmental motor deficits induced by combined fetal exposure to lipopolysaccharide and early neonatal hypoxia/ ischemia: a novel animal model for cerebral palsy in very premature infants. Neuroscience 2009; 158: 673–682. [PubMed: 19010395]
54. Heyes MP, et al.: Different kynurenine pathway enzymes limit quinolinic acid formation by various human cell types. Biochem J 1997; 326:351–356. [PubMed: 9291104]
55. Taylor MW, Feng GS: Relationship between interferon-gamma, indoleamine 2,3-dioxygenase, and tryptophan catabolism. FASEB J 1991;5:2516–2522. [PubMed: 1907934]
56. Widner B, Ledochowski M, Fuchs D: Interferon-gamma-induced tryptophan degradation: neuropsychiatric and immunological consequences. Curr Drug Metab 2000;1:193–204. [PubMed: 11465083]
57. Varma TK, et al.: Endotoxin-induced gamma interferon production: contributing cell types and key regulatory factors. Clin Diagn Lab Immunol 2002; 9: 530–543. [PubMed: 11986256]
58. Robinson CM, Hale PT, Carlin JM: The role of IFN-gamma and TNF-alpha-responsive regulatory elements in the synergistic induction of indoleamine dioxygenase. J Interferon Cytokine Res 2005;25:20–30. [PubMed: 15684619]
59. Kwidzinski E, et al.: Indolamine 2,3-dioxygenase is expressed in the CNS and down-regu-lates autoimmune inflammation. FASEB J 2005;19:1347–1349. [PubMed: 15939737]
60. Liebau C, et al.: Interleukin-12 and interleukin-18 change ICAM-I expression, and enhance natural killer cell mediated cytolysis of human osteosarcoma cells. Cytokines Cell Mol Ther 2002;7:135–142. [PubMed: 14660053]
61. Taguchi A, et al.: Indoleamine 2,3-dioxygenase 1 is upregulated in activated microglia in mice cerebellum during acute viral encephalitis. Neurosci Lett 2014;564:120–125. [PubMed: 24530381]
62. Hoshi M, et al.: Marked increases in hippocampal neuron indoleamine 2, 3-dioxygenase via IFN-gamma-independent pathway following transient global ischemia in mouse. Neurosci Res 2009;63:194–198. [PubMed: 19121343]
63. Pellegrin K, et al.: Enhanced enzymatic degradation of tryptophan by indoleamine 2,3-dioxygenase contributes to the tryptophan-deficient state seen after major trauma. Shock 2005; 23: 209–215. [PubMed: 15718917]
64. Brummelte S, et al.: Developmental changes in serotonin signaling: Implications for early brain function, behavior and adaptation. Neuroscience 2017;342:212–231. [PubMed: 26905950]
65. Vasquez-Vivar J, et al.: Tetrahydrobiopterin in the prevention of hypertonia in hypoxic fetal brain. Ann Neurol 2009;66:323–331. [PubMed: 19798726]
66. Yu L, et al.: Developmental susceptibility of neurons to transient tetrahydrobiopterin insufficiency and antenatal hypoxia-ischemia in fetal rabbits. Free Radic Biol Med 2014;67: 426–436. [PubMed: 24316196]

67. Ichinose H, Nomura T, Sumi-Ichinose C: Metabolism of tetrahydrobiopterin: its relevance in monoaminergic neurons and neurological disorders. Chem Rec 2008; 8: 378–385. [PubMed: 19107867]
68. Guidetti P, et al.: Mitochondrial aspartate aminotransferase: a third kynurenate-producing enzyme in the mammalian brain. J Neuro-chem 2007;102:103–111.
69. Oxenkrug GF: Genetic and hormonal regulation of tryptophan kynurenine metabolism: implications for vascular cognitive impairment, major depressive disorder, and aging. Ann NY Acad Sci 2007;1122:35–49. [PubMed: 18077563]
70. Sas K, et al.: Mitochondria, metabolic disturbances, oxidative stress and the kynurenine system, with focus on neurodegenerative disorders. J Neurol Sci 2007;257:221–239. [PubMed: 17462670]
71. Ting KK, Brew BJ, Guillemin GJ: Effect of quinolinic acid on human astrocytes morphology and functions: implications in Alzheimer's disease. J Neuroinflammation 2009; 6: 36. [PubMed: 20003262]
72. Lapin IP, et al.: Anticonvulsant activity of melatonin against seizures induced by quino-linate, kainate, glutamate, NMDA, and pen-tylenetetrazole in mice. J Pineal Res 1998;24: 215–218. [PubMed: 9572530]
73. Schurr A, West CA, Rigor BM: Neurotoxicity of quinolinic acid and its derivatives in hypoxic rat hippocampal slices. Brain Res 1991; 568: 199–204. [PubMed: 1687668]
74. Jhamandas K, et al.: Quinolinate-induced cortical cholinergic damage: modulation by tryptophan metabolites. Brain Res 1990;529:185–191. [PubMed: 2149296]
75. Baverel G, Martin G, Michoudet C: Glutamine synthesis from aspartate in guinea-pig renal cortex. Biochem J 1990;268:437–442. [PubMed: 2363682]
76. Tavares RG, et al.: Quinolinic acid stimulates synaptosomal glutamate release and inhibits glutamate uptake into astrocytes. Neurochem Int 2002;40:621–627. [PubMed: 11900857]
77. Jamwal S, et al.: Protective effect of spermidine against excitotoxic neuronal death induced by quinolinic acid in rats: possible neurotransmitters and neuroinflammatory mechanism. Neurotox Res 2015;28:171–184. [PubMed: 26078029]
78. Rios C, Santamaria A: Quinolinic acid is a potent lipid peroxidant in rat brain homogenates. Neurochem Res 1991;16:1139–1143. [PubMed: 1686636]
79. Santamaria A, et al.: Quinolinic acid induces oxidative stress in rat brain synaptosomes. Neuroreport 2001;12:871–874. [PubMed: 11277599]
80. Braidy N, et al.: Mechanism for quinolinic acid cytotoxicity in human astrocytes and neurons. Neurotox Res 2009;16:77–86. [PubMed: 19526301]
81. Pierozan P, et al.: Acute intrastriatal administration of quinolinic acid provokes hyperphosphorylation of cytoskeletal intermediate filament proteins in astrocytes and neurons of rats. Exp Neurol 2010;224:188–196. [PubMed: 20303347]
82. Rahman A, et al.: The excitotoxin quinolinic acid induces tau phosphorylation in human neurons. PLoS One 2009;4:e6344. [PubMed: 19623258]
83. Guillemin GJ: Quinolinic acid: neurotoxicity. FEBS J 2012;279:1355. [PubMed: 22251552]
84. Hardingham GE. Do KQ: Linking early-life NMDAR hypofunction and oxidative stress in schizophrenia pathogenesis. Nat Rev Neu-rosci 2016;17:125–134.
85. Potter MC, et al.: Reduction of endogenous kynurenic acid formation enhances extracellular glutamate, hippocampal plasticity, and cognitive behavior. Neuropsychopharmacology 2010;35:1734–1742. [PubMed: 20336058]
86. Bonnin A, et al.: A transient placental source of serotonin for the fetal forebrain. Nature 2011;472:347–350. [PubMed: 21512572]
87. Bonnin A, Levitt P: Fetal, maternal, and placental sources of serotonin and new implications for developmental programming of the brain. Neuroscience 2011;197:1–7. [PubMed: 22001683]
88. Cote F, et al.: Maternal serotonin is crucial for murine embryonic development. Proc Natl Acad Sci USA 2007;104:329–334. [PubMed: 17182745]
89. Yavarone MS, et al.: Serotonin uptake in the ectoplacental cone and placenta of the mouse. Placenta 1993;14:149–161. [PubMed: 8506248]

90. Mackler AM, et al.: Indoleamine 2,3-dioxygenase is regulated by IFN-gamma in the mouse placenta during *Listeria monocytogenes* infection. J Immunol 2003; 170:823–830. [PubMed: 12517946]

91. Goeden N, et al.: Maternal inflammation disrupts fetal neurodevelopment via increased placental output of serotonin to the fetal brain. J Neurosci 2016;36:6041–6049. [PubMed: 27251625]

92. Jansson T: Amino acid transporters in the human placenta. Pediatr Res 2001;49:141–147. [PubMed: 11158505]

93. Mancuso R, et al.: Indoleamine 2,3 dioxygenase (IDO) expression and activity in relapsing-remitting multiple sclerosis. PLoS One 2015;10:e0130715. [PubMed: 26110930]

94. Terness P, et al.: Inhibition of allogeneic T cell proliferation by indoleamine 2,3-dioxygenase-expressing dendritic cells: mediation of suppression by tryptophan metabolites. J Exp Med 2002;196:447–457. [PubMed: 12186837]

95. Mellor AL, et al.: Prevention of T cell-driven complement activation and inflammation by tryptophan catabolism during pregnancy. Nat Immunol 2001;2:64–68. [PubMed: 11135580]

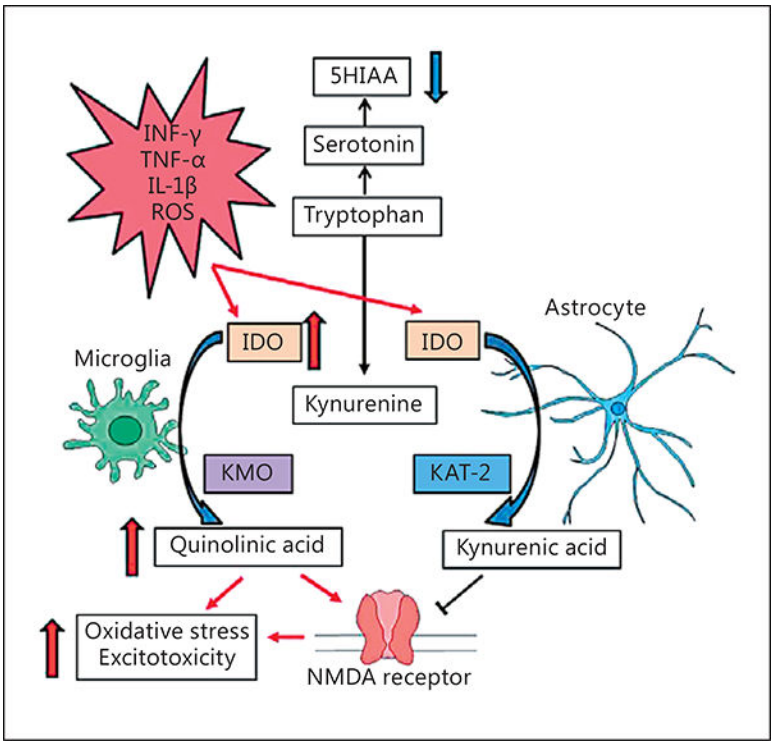

Fig. 1.

Schematic diagram of the KYN pathway in the brain. TRP that enters the brain from the peripheral circulation is converted into KYN by IDO in both the astrocytes and microglia, or into serotonin and its metabolites. Proinflammatory cytokines (e.g., IFN-γ, TNF-α, and IL-lβ) can upregulate IDO expression. KYN is converted into kynurenic acid via KAT-2 located in astrocytes, or converted into QUIN via KMO located in microglia cells. Kynurenic acid is an NMDA receptor antagonist, which can prevent excito-toxicity, whereas QUIN is an NMDA receptor agonist, which can lead to excitotoxicity and increased oxidative stress.

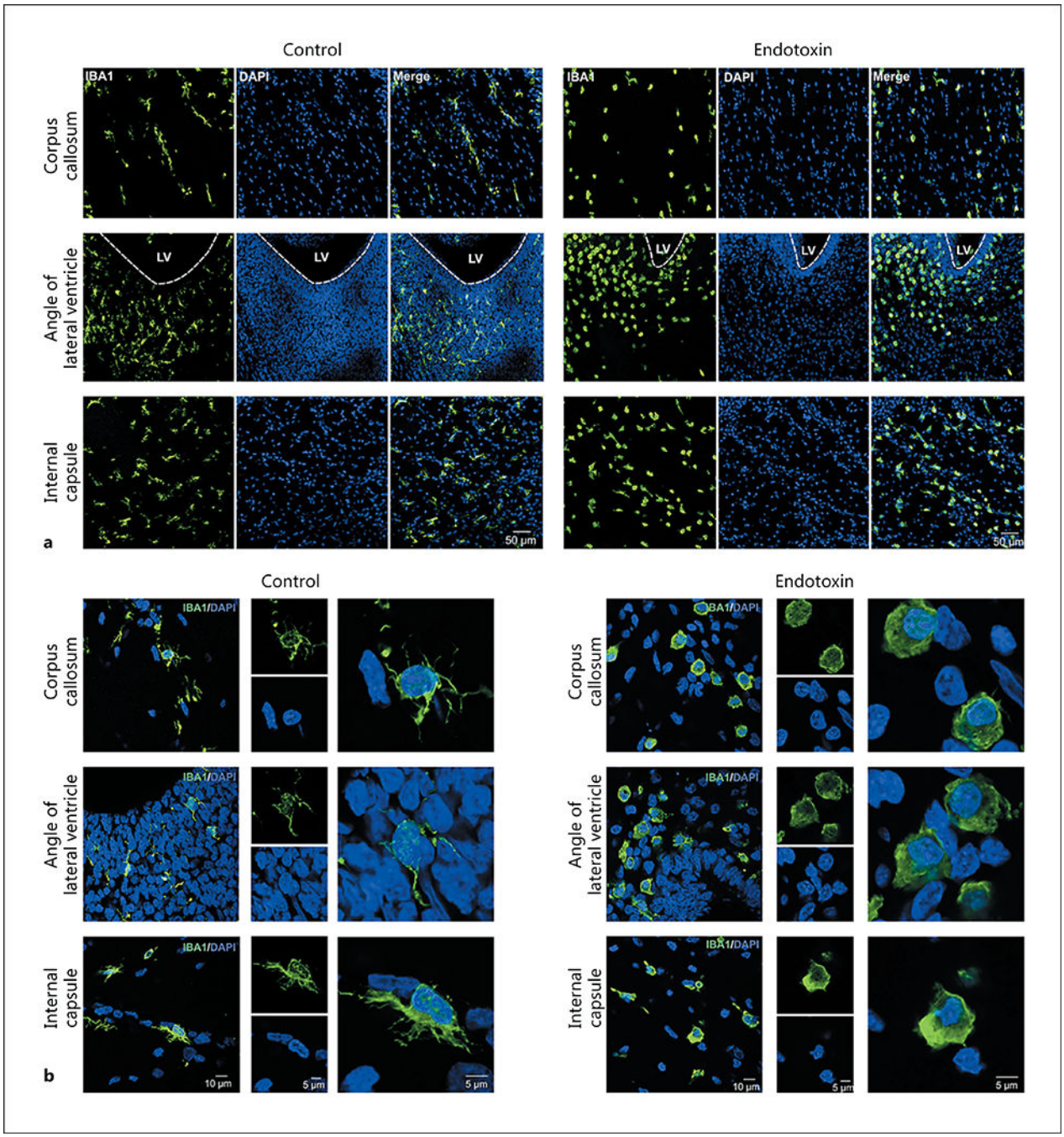

Fig. 2.

In utero endotoxin exposure increased microglial activation in the PVR. **a** Microglia/macrophages were labeled with Iba1, and the staining patterns indicated that in utero endotoxin exposure increased microglia/macrophage activation in the periventricular regions, including the corpus callosum, the angle of the lateral ventricle, and the internal capsule, compared with controls. **b** The activated microglia/macrophages showed an amoeboid shape and retracted and thickened branches compared with the controls. LV, lateral ventricle.

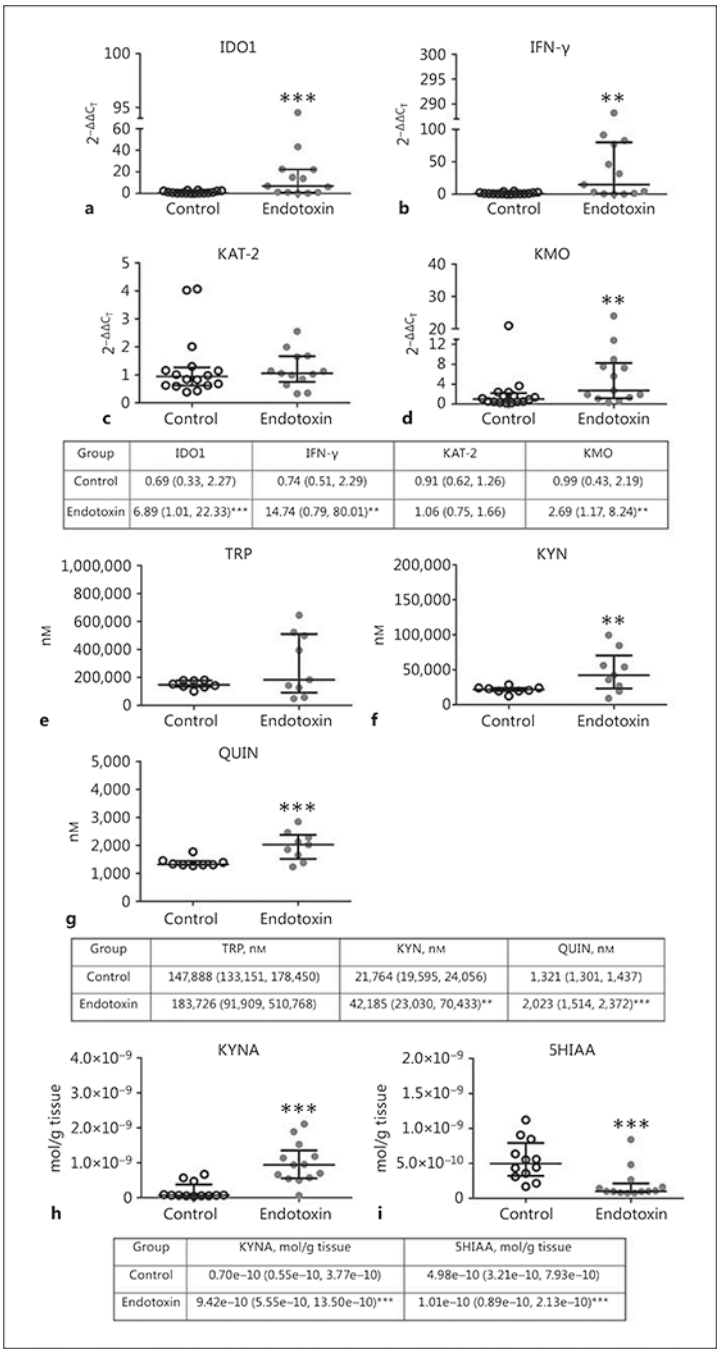

Group	IDO1	IFN-γ	KAT-2	KMO
Control	0.69 (0.33, 2.27)	0.74 (0.51, 2.29)	0.91 (0.62, 1.26)	0.99 (0.43, 2.19)
Endotoxin	6.89 (1.01, 22.33)***	14.74 (0.79, 80.01)**	1.06 (0.75, 1.66)	2.69 (1.17, 8.24)**

Group	TRP, nM	KYN, nM	QUIN, nM
Control	147,888 (133,151, 178,450)	21,764 (19,595, 24,056)	1,321 (1,301, 1,437)
Endotoxin	183,726 (91,909, 510,768)	42,185 (23,030, 70,433)**	2,023 (1,514, 2,372)***

Group	KYNA, mol/g tissue	5HIAA, mol/g tissue
Control	0.70e−10 (0.55e−10, 3.77e−10)	4.98e−10 (3.21e−10, 7.93e−10)
Endotoxin	9.42e−10 (5.55e−10, 13.50e−10)***	1.01e−10 (0.89e−10, 2.13e−10)***

Fig. 3.

TRP pathway metabolites and enzymes in the periventricular white matter region (PVR) of the fetal brain. **a-d** mRNA expression of the major enzymes in the TRP pathway. Kits from the control and endotoxin groups were sacrificed at G29. After perfusion, the PVR were harvested. In utero endotoxin exposure significantly increased the IDO1 (**a**) and IFN-γ (**b**) mRNA expression in the endotoxin kits. **c** There were no significant changes in the KAT-2 mRNA expression. **d** There was a significant upregulation of KMO mRNA expression in the endotoxin kits. **e-g** Metabolites were measured in the PVR by GCMS. **e** There was no

significant difference in the TRP level between the control and endotoxin kits. KYN levels (**f**) and QUIN levels (**g**) were significantly increased in the endotoxin kits. KYNA (**h**) and 5HIAA (**i**) levels were measured by HPLC in the PVR. **h** The KYNA level was significantly increased in the endotoxin kits. **i** 5HIAA (a preserotonin metabolite) was significantly decreased in the PVR of the endotoxin group. Tables are presented as medians with interquartile ranges. * $p < 0.05$, ** $p < 0.01$, *** $p < 0.001$, compared to the controls.

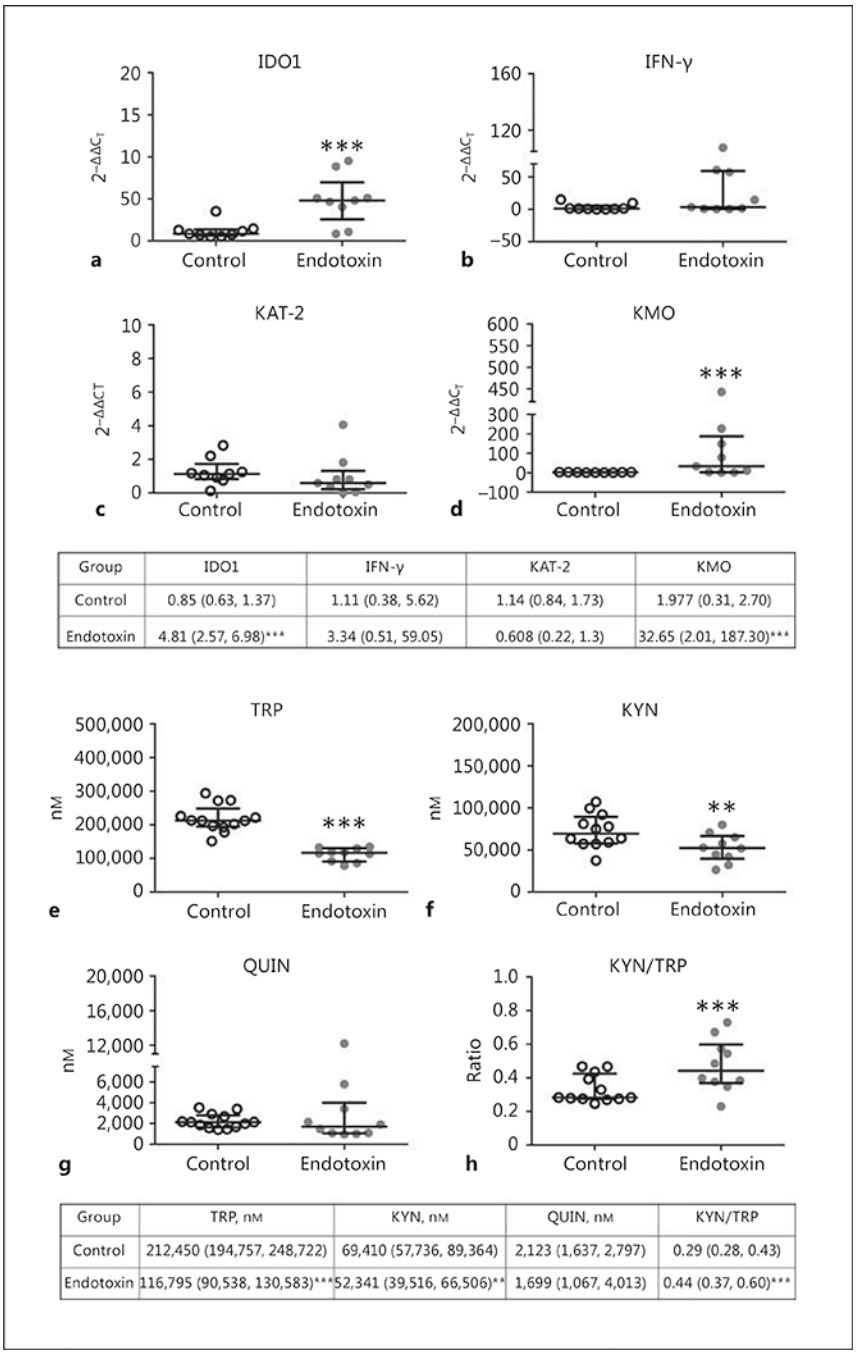

Group	IDO1	IFN-γ	KAT-2	KMO
Control	0.85 (0.63, 1.37)	1.11 (0.38, 5.62)	1.14 (0.84, 1.73)	1.977 (0.31, 2.70)
Endotoxin	4.81 (2.57, 6.98)***	3.34 (0.51, 59.05)	0.608 (0.22, 1.3)	32.65 (2.01, 187.30)***

Group	TRP, nM	KYN, nM	QUIN, nM	KYN/TRP
Control	212,450 (194,757, 248,722)	69,410 (57,736, 89,364)	2,123 (1,637, 2,797)	0.29 (0.28, 0.43)
Endotoxin	116,795 (90,538, 130,583)***	52,341 (39,516, 66,506)**	1,699 (1,067, 4,013)	0.44 (0.37, 0.60)***

Fig. 4.

TRP pathway metabolites and enzymes in the placenta. **a-d** mRNA expression of the major enzymes in the TRP pathway. **a** In utero endotoxin exposure significantly increased IDO1 mRNA expression in the placenta. There was no significant change in the IFN-γ (**b**) and KAT-2 (**c**) mRNA expression. **d** There was a significant increase in KMO mRNA expression in the endotoxin-treated placenta. **e-h** Metabolites were measured in the placenta by GCMS after perfusion. Both TRP levels (**e**) and KYN levels (**f**) were significantly decreased in the endotoxin-exposed placenta when compared to controls. **g** There was no significant change

in the QUIN levels between control and endotoxin-treated placentas. **h** The KYN/TRP ratio was significantly higher in the endotoxin-treated placenta. Tables are presented as medians with interquartile ranges. * $p < 0.05$, ** $p < 0.01$, *** $p < 0.001$, compared to the controls.

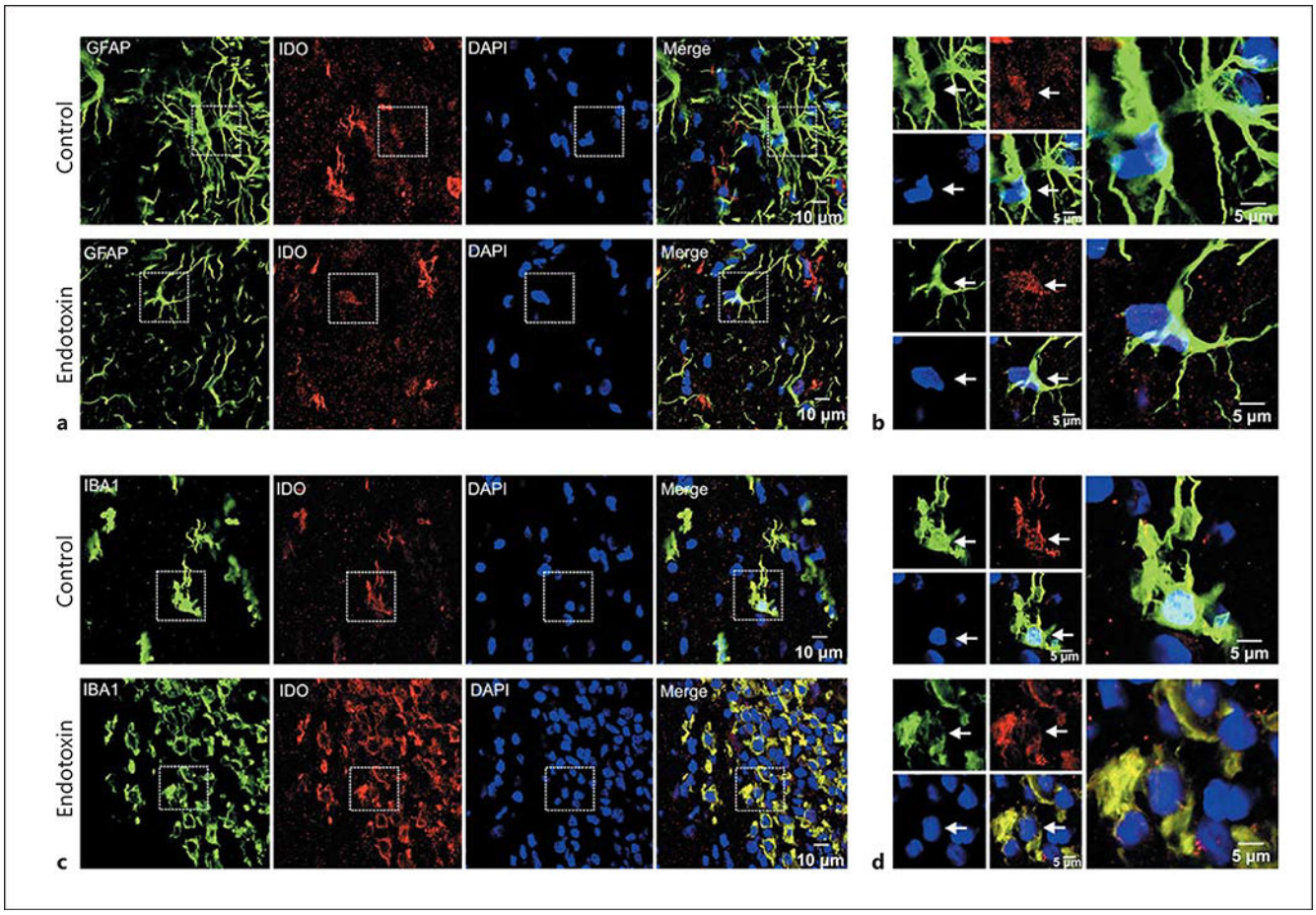

Fig. 5.

IDO colocalizes with astrocytes and microglia in the PVR of control and endotoxin kits. **a, b** Colocalization of GFAP/IDO. **a** Representative GFAP and IDO costaining images from control and endotoxin kits at G29. **b** The high magnification images are indicated by the box in **a. c, d** Colocalization of IBA1/IDO. **c** Representative IBA1 and IDO costaining images from control and endotoxin kits at G29. **d** The high magnification images are indicated by the box in **c.** Arrows indicate some of the colocalization areas.

Table 1.

Primers used for real-time PCR

Gene	Forward primer	Reverse primer
KMO	GTA GGA TGT GAT GGA GCC TAT TC	CTC CAT GTA TCC GTG AGG AAT G
IDO1	GGA GAC ATC CGA AAG GTC TTG	CAG TCA GCA TAC ACG AGA ATA GG
KAT-2	GTC CCA AAT CGC AAC AAC CC	ACA CGC CCA TCA ACA TCC AT
IFN-γ	TGT CCA GTT GCT GCC TAT TT	CAG AGG ACA AGG TCA CAT CAC
TPH	CTTTGCAGACTCGGCTATGA	TTGTTGAGCTCCCGGAATAC
TDO	CATGAGTGGGTGCCCATATT	GTCTTCGTCCCTGCTTTCTAC
GAPDH	TGA CGA CAT CAA GAA GGT CGT G	GAA GGT GGA GGA GTG GGT GTC

KMO, kynurenine monooxygenase; IDO, indoleamine 2,3-dioxygenase; TDO, tryptophan 2,3-dioxygenase; KAT, kynurenine amino transferase; IFN-γ, interferon gamma; GAPDH, glyceraldehyde 3-phosphate dehydrogenase.